Repression of lysosomal transcription factors Tfeb and Tfe3 is essential for the development and function of microglia

Harini Iyer[1], Kimberle Shen[1,#], Ana M. Meireles[1], William S. Talbot[1,*]

[1]Department of Developmental Biology, Stanford University School of Medicine, Stanford CA 94305
[#]Present address: Genentech Inc, 1 DNA Way, South San Francisco, CA 94080
[*]Corresponding author: william.talbot@stanford.edu

SUMMARY

As the primary phagocytic cells of the central nervous system, microglia exquisitely regulate their lysosomal activity to facilitate brain development and homeostasis. However, mechanisms that coordinate lysosomal activity with microglia development, migration, and function remain unclear. Here we show that embryonic macrophages require the lysosomal GTPase RagA and the GTPase-activating protein Folliculin (Flcn) for colonization of the brain. Mutants lacking RagA and Flcn have nearly identical phenotypes, suggesting that RagA and Flcn act in concert in developing microglia. Furthermore, we demonstrate that RagA and Flcn repress the key lysosomal transcription factor Tfeb, and its homologs Tfe3a and Tfe3b, in macrophages. Accordingly, defects in *rraga* mutants can be restored by simultaneous mutations in *tfeb, tfe3a,* and *tfe3b*, and overexpression of *tfe3b* in the macrophage lineage recapitulates the major defects observed in *rraga* and *flcn* mutants. Collectively, our data define a lysosomal regulatory circuit that is essential for early development of microglia.

INTRODUCTION

Microglia, the primary resident macrophages of the central nervous system, govern multiple aspects of brain architecture and function. During development, microglia promote synapse formation and maturation, stimulate neurogenesis, and eliminate excess or apoptotic cells (Cunningham et al., 2013; Schafer et al., 2012; Shigemoto-Mogami et al., 2014; Wakselman et al., 2008). To maintain adult brain homeostasis,

microglia surveil the brain for aberrations, mediate repair and regeneration, and facilitate immune clearance of pathogens and cellular debris (Davalos et al., 2005; De Biase et al., 2017; Hagemeyer et al., 2017; Matcovitch-Natan et al., 2016; Nimmerjahn et al., 2005; Sierra et al., 2010). As professional phagocytic cells, nearly all these activities of microglia require lysosomes for either degradation of engulfed material or mounting an immune response. Moreover, many studies have found a correlation between aberrant microglial activity associated with neurodegeneration and lysosomal dysregulation (Holtman et al., 2015; Plaza-Zabala et al., 2017; Sole-Domenech et al., 2016). Much less is known about the mechanisms that regulate lysosomes during microglia development. A better understanding of genes regulating lysosomal function during development and homeostasis has the potential to illuminate how these critical organelles might be disrupted during aging and disease.

Central to lysosomal functions are Transcription factor EB (Tfeb) and other members of the Microphthalmia-associated transcription factor (MiTF) protein family. In cell culture and some cell types in vivo, Tfeb, and the related transcription factor Tfe3, have been reported to activate diverse lysosomal processes, such as lysosomal biogenesis, autophagy, and exocytosis (Napolitano and Ballabio, 2016; Palmieri et al., 2011; Sardiello et al., 2009; Settembre et al., 2011; Settembre et al., 2013). In recent years, there has been an increasing appreciation of the dysregulation of Tfeb in neurodegenerative diseases (Cortes et al., 2014; Decressac et al., 2013; Martini-Stoica et al., 2016; Reddy et al., 2016; Tsunemi et al., 2012), which has led to attempts at enhancing cellular clearance by overexpressing Tfeb to activate autophagy and

lysosomal pathways in cell culture or animal models of neurodegeneration (Dehay et al., 2010; Parr et al., 2012; Pickrell and Youle, 2015; Polito et al., 2014; Tsunemi et al., 2012; Xiao et al., 2014; Xiao et al., 2015). Although exogenous expression of Tfeb has been shown to improve behavioral deficits and reduce pathology due to misfolded proteins in some models of neurodegenerative diseases (Polito et al., 2014; Xiao et al., 2014; Xiao et al., 2015), the identity of cells that must overexpress Tfeb to generate these beneficial effects is unclear. Furthermore, the role of Tfeb in microglia, cells that depend on lysosomal pathways for executing many of their functions, is unknown.

The importance of investigating the development and function of microglia in vivo is evident from experiments showing that microglia rapidly lose their transcriptional and epigenetic identity when separated from their niche (Amit et al., 2016; Bohlen et al., 2017; Butovsky et al., 2014; Gosselin et al., 2014; Gosselin et al., 2017). Accordingly, studies of microglia in zebrafish using live imaging and mutational studies have led to many important insights into the development and function of these critical cells (Casano et al., 2016; Meireles et al., 2014; Peri and Nusslein-Volhard, 2008; Shiau et al., 2013; Wu et al., 2018; Xu et al., 2015). Here we capitalize on the experimental advantages of zebrafish to functionally define a lysosomal regulatory circuit that is essential in development and function of microglia. We show that lysosomal GTPase RagA (encoded by *rraga*) is necessary for the normal development, migration, and function of both early microglia and peripheral macrophages. We provide genetic evidence that the lysosomal GTPase activating protein Folliculin is functionally coupled to RagA in macrophages and microglia. Furthermore, we demonstrate that the

simultaneous loss of *tfeb* and *tfe3* (including both zebrafish paralogs of *tfe3, tfe3a* and *tfe3b*) is sufficient to restore microglia numbers in *rraga* and *flcn* mutants, indicating that RagA and Flcn must repress these key lysosomal transcription factors for normal development of microglia. Moreover, we find that overexpression of *tfe3b* in the macrophage lineage phenotypically recapitulates all microglia and macrophage defects we observe in *rraga* and *flcn* mutants. Together, our observations reveal a lysosomal pathway that regulates development and function of microglia and macrophages. Additionally, our observation that Tfeb and Tfe3 must be repressed for normal development of microglia has important implications for therapeutic strategies that modulate Tfeb activity in the context of neurodegeneration.

RESULTS

Embryonic macrophages fail to colonize the brain in *rraga* mutants

We have previously shown that the lysosomal GTPase RagA (encoded by *rraga*) is necessary for the development of microglia in zebrafish (Shen et al., 2016). *rraga* mutants have fewer microglia compared to their wildtype siblings and the remaining microglia display an abnormal morphology and a reduced capacity to digest neuronal debris (Shen et al., 2016). As early as 3 days post fertilization (dpf), *rraga* mutants have fewer microglia than wildtype embryos, as indicated by reduced expression of *apoe* and *slc7a7* (Peri and Nusslein-Volhard, 2008; Rossi et al., 2015; Shen et al., 2016). Previous studies have not, however, addressed the developmental timing or cause of

this reduction in microglial cell number in *rraga* mutants. To define the disrupted developmental processes underlying the *rraga* mutant phenotype, we first examined the specification of embryonic macrophages that give rise to microglia. In zebrafish, microglial progenitors are specified in the anterior paraxial mesoderm starting around 14 hours post fertilization (hpf); these embryonic macrophages migrate across the yolk to accumulate in the rostral blood island (RBI), located in the anterior region of the yolk, by approximately 22 hpf (Herbomel et al., 1999, 2001). Previous studies have shown that embryonic macrophages from the RBI colonize the brain initially between 2 and 3 dpf (Wu et al., 2018; Xu et al., 2016) and they begin to express microglia-specific genes by 3 dpf (Peri and Nusslein-Volhard, 2008). To investigate the development of embryonic macrophages, a population that includes progenitors of microglia, in *rraga* mutants, we quantified these cells in embryos between 24 and 26 hpf, using the *Tg(mpeg:GFP)* transgene, which expresses green fluorescent protein in the macrophage lineage (Ellett et al., 2011). We observed no significant difference in the number of GFP-labeled cells between *rraga* mutants and their wildtype siblings either in the yolk (Figures 1A, 1B) or the rest of the body (Figures 1A, 1C), indicating that specification and migration of embryonic macrophages is normal at this stage in *rraga* mutants.

To define the developmental window during when reduction of microglia numbers becomes apparent in *rraga* mutants, we quantified macrophages in the dorsal brain, where microglia are easily visualized, at 2, 2.5, 3, and 5 dpf (Figure 1D). There was a significant reduction in the number of developing microglia in the midbrain of *rraga* mutants at 3 dpf, but not in earlier stages (Figure 1D). To investigate how the

reduction of macrophage numbers in the brain occurs in *rraga* mutants, we performed timelapse imaging starting at 60 hpf and ending at ~78 hpf. Analysis of the timelapse movies showed that fewer macrophages migrate into the brain in *rraga* mutants (Figures 1E-H, Movies S1, S2), consistent with our timecourse experiment (Figure 1D). Furthermore, timelapse imaging provided no evidence for other possibilities, such as reduced proliferation or increased apoptosis in *rraga* mutants (Figures 1E-H, Movies S1, S2) after embryonic macrophages enter the brain. These experiments demonstrate that microglial progenitors in *rraga* mutants fail to migrate into the brain between 2 and 3 dpf.

Peripheral macrophages are disrupted in *rraga* mutants

Previous studies have not examined the extent to which macrophages outside the brain are affected in *rraga* mutants. We used the *Tg(mpeg:GFP)* transgene to visualize macrophages at 2, 2.5, and 3 dpf. In lateral views of the head, the numbers of macrophages were similar between *rraga* mutants and their wildtype siblings at 2 dpf (Figures 1I, 1K, S1E), and *rraga* mutants showed a slight, but insignificant, reduction of macrophages in this region at 2.5 dpf (Figures 1K, S1A, S1E). There was, however, a striking and significant reduction of macrophage numbers in the head in *rraga* mutants by 3 dpf (Figures 1I', 1K, S1E), with very few macrophages remaining in the mutants. In contrast, a large number of macrophages persisted in the trunk and tail regions of *rraga* mutants at all stages we examined up to 8 dpf (Figures 1J-J', 1L, S1B-D), although macrophage numbers were significantly reduced in *rraga* mutants beginning at 2.5 dpf (Figures 1J-J', 1L, S1A, S1E).

The morphology of macrophages and microglia is frequently used as a readout of their functional state; highly ramified microglia are typically thought to be “resting” or “surveilling”, whereas rounded, less motile microglia are considered to be activated in response to infection or injury, or are dysfunctional in some way (Block et al., 2007). At 3 dpf, macrophages in the tail region of *rraga* mutants displayed an abnormal, rounded morphology (Figure 1M), similar to microglia at 4dpf (Shen et al., 2016). Finally, to assess the function of macrophages in *rraga* mutants, we used timelapse imaging to track macrophage movement in response to injury of the tail fin (Figure 1N). Significantly fewer macrophages in *rraga* mutants moved to the wound site at 8 hours after injury (Figure 1N), indicating that macrophages are unable to either sense or respond to injury cues. Together, these observations show that the number, morphology, and function of macrophages are disrupted in *rraga* mutants and that these phenotypes manifest between 2 and 3 dpf. Furthermore, considering the lack of appropriate injury response (Figure 1N), and our observation that macrophages are unable to colonize the brain in *rraga* mutants (1E-H), we conclude that cells of the macrophage lineage in *rraga* mutants are unable to migrate appropriately in response to injury or developmental cues (Casano et al., 2016; Xu et al., 2016).

Simultaneous loss of lysosomal transcription factors *tfeb, tfe3a,* and *tfe3b* rescues microglia numbers in *rraga* mutants

The transcription factor EB (Tfeb) regulates most lysosomal functions including lysosomal biogenesis, autophagy, and exocytosis (Palmieri et al., 2011; Sardiello et al.,

2009; Settembre et al., 2011). Lysosomal activity is especially critical for the function of macrophages and microglia because these cells rely upon lysosomes for their principal activities, including clearing apoptotic debris and mounting immune responses. The role of Tfeb in the development of microglia and macrophages has, however, remained largely unexplored. Furthermore, several lines of evidence indicate that RagA represses Tfeb and other related transcription factors (Napolitano and Ballabio, 2016; Settembre et al., 2013), although the extent to which the RagA-Tfeb lysosomal pathway functions in the macrophage lineage in vivo is unclear.

To address whether RagA represses Tfeb in microglia, we crossed *rraga*$^{+/-}$*; tfeb*$^{+/-}$ double heterozygotes (Meireles et al., 2018), and labeled microglia using neutral red, a dye that preferentially accumulates in microglia (Herbomel et al., 2001). Imaging and quantification of microglia in the dorsal midbrain showed that *rraga* mutants have significantly fewer neutral red-labelled microglia, as shown previously (Shen et al., 2016) (Figure 2A). Simultaneous loss of *tfeb* in the *rraga* mutant background partially restored microglia numbers (Figure 2A, B). These data provided evidence that hyperactivated Tfeb contributes to, but does not solely cause, microglial defects in *rraga* mutants.

One hypothesis for the incomplete rescue we observed in *rraga; tfeb* double mutants is that RagA might also repress members of the Microphthalmia-associated transcription factor (MiTF) family, which consists of Mitf, Tfeb, Tfe3, and Tfec (Napolitano and Ballabio, 2016). The members of this family show significant functional similarity and

redundancy, reflecting their highly conserved DNA-binding domains (Martina et al., 2014). Moreover, Tfeb and Tfe3 have been shown to act cooperatively to regulate cytokine production in the RAW 264.7 macrophage cell line (Pastore et al., 2016), although the extent of functional overlap between these transcription factors in macrophages in vivo remains uncharacterized.

To determine if Tfe3 functions in macrophages and microglia, we generated mutants for the two zebrafish paralogs of *tfe3, tfe3a* and *tfe3b* (Figure S2 and Table S1) (Lister et al., 2011). Briefly, we raised *tfe3a* or *tfe3b* CRISPR-injected fish to adulthood (F0), identified out-of-frame deletion in the genes of their progeny (F1) (Figure S2), and crossed the F1 fish to *rraga*$^{+/-}$ heterozygous adults to generate *rraga; tfe3a* and *rraga; tfe3b* double heterozygotes. Neutral red assay on the progeny of double heterozygous fish revealed that mutations in *tfe3a* (Figures 2C, 2D) or *tfe3b* (Figures 2E, 2F) can partially rescue microglia numbers in *rraga* mutants, much as observed in *rraga; tfeb* double mutants (Figures 2A, 2B). Importantly, the loss of even a single copy of *tfeb, tfe3a,* or *tfe3b* can partially rescue microglia in *rraga* mutants (*rraga*$^{+/-}$*; tfeb*$^{+/-}$ in Figure 2B; *rraga*$^{+/-}$*; tfe3a*$^{+/-}$ in Figure 2D; *rraga*$^{+/-}$*; tfe3b*$^{+/-}$ in Figure 2F), indicating that microglia are highly sensitive to increased levels of each of these transcription factors. Together, these experiments show that RagA is essential to repress Tfeb, Tfe3a, and Tfe3b in microglia.

To further explore the dosage-dependent rescue of Tfeb and Tfe3, as well as to better

understand the extent of functional overlap between Tfeb, Tfe3a, and Tfe3b, we generated *rraga*$^{+/-}$; *tfeb*$^{+/-}$; *tfe3a*$^{+/-}$; *tfe3b*$^{+/-}$ quadruple heterozygous animals. Since *tfeb* and *tfe3b* are present on the same chromosome and are about 2 MB apart on chromosome 11, we injected the *tfe3b* CRISPR into *tfeb*$^{+/-}$ heterozygotes, raised these fish, and crossed them to *rraga*$^{+/-}$ and *tfe3a*$^{+/-}$ lines to obtain quadruple heterozygous fish. Neutral red assay and quantification (Figures 2G-I) revealed that combined loss of a single copy of *tfeb, tfe3a,* and *tfe3b* was sufficient to completely restore microglia numbers in *rraga* mutants (Figure 2H). We also observed a full rescue of microglia in *rraga* mutants when 4, 5, or 6 copies of *tfeb*, *tfe3a,* and *tfe3b* were mutated (Figures 2H, 2I). Despite the functions of Tfeb and Tfe3 in regulating lysosomal genes and the role of lysosomes in critical functions of microglia, we did not observe any obvious defects in microglia in *tfeb, tfe3a,* or *tfe3b* mutants alone (Figures 2A-F), or in combination, including *tfeb; tfe3a; tfe3b* triple mutants (Figures 2G-I). Collectively, these observations indicate that RagA represses Tfeb, Tfe3a, and Tfe3b in microglia, that hyperactivity of these transcription factors causes the microglia defects in *rraga* mutants, and that *tfeb* and its homologs are not required for normal microglial development.

***folliculin* and *rraga* mutants have similar phenotypes**

Several studies link the protein Folliculin (Flcn) to the repression of Tfe3 (Hong et al., 2010; Li et al., 2019; Wada et al., 2016), and in some cases, Tfeb (El-Houjeiri et al., 2019); however, the mechanism through which Flcn regulates the nuclear translocation Tfe3 (or Tfeb) is not fully understood. Some studies propose that FLCN, along with its

binding partners, serves as a GTPase activating protein (GAP) for RAGC/D, thereby activating mTORC1, which in turn can repress TFEB and TFE3 through phosphorylation in certain contexts (Ferguson, 2015; Tsun et al., 2013). Other studies suggest that FLCN may serve as a guanine exchange factor (GEF) for RAGA/B, although such GEF activity has not been demonstrated (Nookala et al., 2012; Petit et al., 2013).

To assess the functional interaction between Flcn and RagA in vivo, we generated *flcn* mutants using CRISPR-Cas9 (Figure S3A). We found that mutations in *flcn* or *rraga* caused a strikingly similar phenotype in macrophages and microglia. *flcn* mutants have significantly fewer neutral red-labeled microglia in their dorsal midbrain (Figures 3A, S3B), as in the case of *rraga* mutants (Figure 2) (Shen et al., 2016). Furthermore, this reduction in microglia numbers in *flcn* mutants was rescued by simultaneous loss of *tfeb* and *tfe3b* (Figure 3A) and partially rescued in *flcn; 3a* double mutants (Figure S3B). Once again, as in the case of *rraga* (Figure 2), we observed a dosage-dependent effect, and *flcn* mutants that are heterozygous for the *tfeb; tfe3b* double mutant chromosome or *tfe3a* display a partial, intermediate level of rescue of microglia number in the neutral red assay (Figures 3A, S3B). We also used the dye LysoTracker Red (Peri and Nusslein-Volhard, 2008) to examine the morphology of acidic compartments within microglia in *rraga* or *flcn* mutants. As shown previously (Shen et al., 2016), *rraga* mutants have a significant expansion of LysoTracker Red punctae in microglia (Figure 3B); we found that this expansion is partially rescued in *rraga; tfe3a* double mutants (Figure 3B). Remarkably similar to *rraga* mutants, we also found that *flcn* mutants had enlarged LysoTracker Red punctae in their microglia and that this expansion is fully

rescued in *flcn; tfeb; tfe3b* triple mutants (Figure 3C). *rraga* mutants have very few *apoe*-expressing microglia in their dorsal midbrain (Shen et al., 2016) (Figure 3D), and we found that this defect is partially rescued in *rraga; tfe3a* double mutants (Figure 3D). Similarly, there was a strong reduction in *apoe*-expressing microglia in *flcn* mutants and this defect was rescued in *flcn; tfeb; tfe3b* triple mutants (Figure 3E).

Finally, we examined these genotypes using the *Tg(mpeg:GFP)* line to assess the morphology of microglia and macrophages. Both *rraga* and *flcn* displayed abnormal, rounded morphology of microglia and macrophages (Figures 3F, 3G), a defect that was at least partially restored in *rraga; tfe3a* mutants (Figure 3F) and *flcn; tfeb; tfe3b* mutants (Figure 3G). In sum, our experiments show that the key lysosomal proteins Flcn and RagA have very similar functions in microglia and macrophages in vivo and are both essential to repress Tfeb and Tfe3. Moreover, all known defects observed in the macrophage lineage in *rraga* or *flcn* mutants can be rescued to varying degrees by simultaneous loss of *tfeb* or *tfe3a,* or *tfe3b*.

Overexpression of *tfe3b* in macrophages recapitulates *rraga* mutant phenotypes in microglia and macrophages

We reasoned that if Tfeb and Tfe3 are the primary downstream targets repressed by RagA, then overexpression of Tfeb or Tfe3 in macrophages should recapitulate the *rraga* mutant phenotype. We constructed transgenic fish that overexpressed Tfe3b in cells of the macrophage lineage, *Tg(mpeg:tfe3b; cmlc2:mcherry)*, and found that indeed

these animals had the defects characteristic of *rraga* or *flcn* mutants (Figures 4A-E). First, *Tg(mpeg:tfe3b)* animals have significantly fewer neutral red-labeled microglia than *Tg(mpeg:GFP)* animals (Figure 4A), similar to mutants for *rraga* or *flcn* (Figures 2, 3A, S3B) (Shen et al., 2016). Second, animals that overexpress *tfe3b* in macrophages have significantly enlarged LysoTracker Red punctae in microglia (Figure 4B), as observed in *rraga* or *flcn* mutants (Figures 3B, 3C). Third, *Tg(mpeg:tfe3b)* animals had reduced *apoe* labeling in the dorsal midbrain (Figure 4C), once again similar to both *rraga* and *flcn* mutants (Figures 3D, 3E) (Shen et al., 2016), and in contrast to *Tg(mpeg:GFP)* controls (Figure 4E). Finally, by crossing *Tg(mpeg:tfe3b)* animals to the *Tg(mpeg:GFP)* fish, we found that animals overexpressing *tfe3b* in the macrophage lineage had fewer microglia and macrophages, and that the remaining cells exhibited abnormal, rounded morphology (Figures 4D, 4E), similar to *rraga* (Figures 1M, 3F) (Shen et al., 2016) or *flcn* (Figure 3G) mutants. These experiments demonstrate that the overexpression of *tfe3b* is sufficient to recapitulate the *rraga* mutant phenotype in microglia and macrophages (Figures 4A-E). Collectively, our data indicate that the primary essential function of RagA and Flcn in macrophages is to repress Tfeb and Tfe3.

DISCUSSION

Our experiments demonstrate that a lysosomal regulatory circuit, involving the GTPase RagA, the GTPase activating protein Flcn, and the transcription factors Tfeb, Tfe3a, and Tfe3b, is essential for the development and function of microglia and macrophages. In *rraga* mutants, Tfeb, Tfe3a, and Tfe3b are hyperactivated, which in

turn disrupts the migration of embryonic macrophages and reduces the ability of microglia to digest apoptotic cell debris. Microglia and macrophages depend on lysosomal pathways to execute their phagocytic functions, and previous studies show that activation of Tfeb and Tfe3 increases lysosomal gene expression (Sardiello et al., 2009; Settembre et al., 2011). It is therefore seemingly paradoxical that microglia and macrophages appear normal in *tfeb; tfe3a; tfe3b* triple mutants. Some studies indicate that cellular stresses, such as endoplasmic reticulum stress or starvation, can activate Tfeb and Tfe3 (Martina et al., 2016; Martina and Puertollano, 2017; Raben and Puertollano, 2016). Accordingly, we propose that Tfeb and Tfe3 may activate lysosomal pathways in the macrophage lineage only under conditions of stress, for example, cellular stress resulting from injury or misfolded proteins. Thus, RagA and Flcn could be required to regulate the levels or activity of Tfeb and Tfe3 - and restore homeostasis to the cell - after stresses that activate these transcription factors have been alleviated. Furthermore, recent studies have reported that developmental disorders are caused by mutations in *TFE3* (Kaplanis et al., 2020; Villegas et al., 2019). Some of these mutations constitutively activate TFE3 by disrupting the ability of RAG proteins to repress TFE3, implicating hyperactivation of TFE3 as the potential cause of the developmental disorders (Villegas et al., 2019). Our current observations, demonstrating that RagA represses Tfeb and Tfe3 in microglia, together with previous studies indicating a similar antagonistic relationship between RagA and Tfeb in oligodendrocytes (Meireles et al., 2018), indicates that disruption of Tfeb and Tfe3 in these critical glial cells may contribute to developmental disorders in these patients.

Finally, our experiments reveal that Tfeb and Tfe3 must be repressed for early development of microglia, but it is unclear why hyperactivation of Tfeb and Tfe3 leads to migration defects in microglia. In addition, much less is known about the regulation of these transcription factors in the maintenance and function of adult microglia (Ferrero et al., 2018; Mazzolini et al., 2019; Xu et al., 2015). Future studies aiming to understand the regulation and functions of Tfeb and Tfe3 in microglia during development and aging will not only broaden our understanding of lysosomal pathways in these essential glial cells, but will also inform therapeutic strategies aimed at modulating Tfeb activity in neurodegeneration and other diseases.

MATERIALS AND METHODS

Zebrafish lines

Embryos from wildtype (TL or AB) strains and *Tg(mpeg:GFP)* transgenic line (Ellett et al., 2011) were raised at 28.5 ºC methylene blue embryo water. For all imaging experiments, embryos were treated with 0.003% 1-phenyl-2-thiourea (PTU) to inhibit pigmentation, and anesthetization was done using .016% MS-222 (Tricaine) prior to experimental procedures. For neutral red assay, methylene blue was excluded from embryo water. All animal protocols have been approved by the Stanford Institutional Animal Care and Use Committee.

Generation of *tfe3a, tfe3b,* and *flcn* mutants with CRISPR-Cas9

sgRNAs targeting *tfe3a*, *tfe3b,* and *flcn* were designed using CHOPCHOP (https://chopchop.cbu.uib.no/) (Labun et al., 2016; Montague et al., 2014). Oligonucleotides containing T7 binding site and the CRISPR sequence were annealed to tracrRNA template. Assembled oligonucleotides were transcribed using HiScribe T7 Quick (NEB, E2050S) kit. Following DNase treatment, the RNA was purified using mirVana miRNA isolation kit (Invitrogen, AM1561). An aliquot of the sgRNA eluate was run on agarose gel and quantified using NanoDrop 8000. CRISPR injections were performed at 1-cell stage. Injection mix consisted of 300 ng/µl of Cas9 protein (Macrolab, Berkeley, http://qb3.berkeley.edu/macrolab/cas9-nls-purified-protein/) and 300 ng/µl of the sgRNA in Tris-HCl (pH 7.5). A small amount of phenol red was added to the mix to help with visualization during injection. Injected fish were raised to adulthood.

The F1 progeny of F0-injected fish were screened for an out-of-frame insertions or deletions. Details of guideRNAs used, lesions, and restriction enzyme assays for genotyping mutants are described in Table S1. The *tfe3a* allele, *st124,* is a 2 bp deletion in exon 2. We used two mutant alleles of *tfe3b: st125,* a 25 bp deletion in exon 2, and *st126,* which is linked to *tfeb* (*st120),* and is a 2 bp deletion in exon 2. The *flcn* mutant has two different lesions generated by co-injecting two guide RNAs: *st127* is a 7 (-8+1) bp change in exon 2 (which disrupts the open reading frame), followed by a 4 bp deletion in exon 7, approximately 10,000 kb downstream of *st127*.

Neutral red assay

Neutral red was dissolved in distilled water to give a 2.5 mg/ml stock solution, which is stable at room temperature for several months. Staining using neutral red was done by treating larvae at 4 dpf with 5 µg/ml solution of neutral red in embryo water containing PTU for 3 hours (Herbomel et al., 2001). Animals were rinsed at least twice after neutral red staining and washed overnight in embryo water with PTU at 28.5 ºC. Approximately 24 hours post-neutral red treatment, larvae were anesthetized and mounted in 1.5% low melting point agarose. The number of neutral red^{+} microglia were counted, and images were acquired immediately after counting using Zeiss AxioCam HRc camera with the AxioVision software. Between 100-150 embryos were mounted and imaged for each double, triple, and quadruple mutant experiment. After imaging, all animals were genotyped by PCR and statistical analysis was performed.

LysoTracker Red assay

LysoTracker Red DND-99 (ThermoFisher, L7528) was diluted 1:100 in embryo water+PTU. Larvae at 4 dpf were incubated in the LysoTracker Red solution for 30-45 minutes. After staining, larvae were washed in embryo water containing PTU for 30 minutes, with at least 3 washes approximately 8-10 minutes apart. Following anesthesia and mounting in agarose, images were acquired using Zeiss LSM confocal microscope. All genotyping was done by PCR post-imaging and area of LysoTracker Red punctae in

the midbrain, where most microglia are present, was calculated using ImageJ for at least three animals per genotype.

in situ hybridization

apoe antisense probe was generated from a pCRII clone carrying 505 bp of *apoeb* gene (Shiau et al., 2013).

in situ hybridization was performed using standard methods (Thisse and Thisse, 2008). Briefly, embryos at 4 dpf were fixed overnight in 4% paraformaldehyde, dehydrated at least overnight in 100% methanol, rehydrated in PBS-Triton X-100 and PBS, permeabilized using proteinase K (20 mg/ml) at a dilution of 1:1000 for 1 hour, and incubated overnight with antisense riboprobes at 65 ºC. Following washes in 2X and 0.2X SSC, and incubation in MAB block containing 10% normal sheep serum, animals were incubated overnight at 4 ºC in MAB block containing 1:1000 dilution of anti-digoxigenin antibody conjugated to alkaline phosphatase. The following day, after at least 6X20 minute washes in MAB-Triton X-100 buffer, animals were incubated in development solution containing NBT (Roche, 11383213001) and BCIP (11383221001). Development was stopped at the same time for all samples in a single experiment by evaluating the strength of the *apoe* signal in control animals. Animals were washed twice in PBS-Triton X-100, left in 100% ethanol overnight for destaining, and rehydrated in PBSTx. Following genotyping of finclips, representative animals were mounted in 100% glycerol and images were captured using Zeiss AxioCam HRc camera with the

AxioVision software.

Tfe3b overexpression construct and injection

Full length *tfe3b* (accession number: NM_001045066.1) was cloned from wild type cDNA into pCR8 vector and verified by Sangar sequencing. Macrophage-specific expression vector was assembled using multisite Gateway method using the *mpeg* promoter and a destination vector containing Tol2-transposon sites for genomic integration and *Tg(cmlc2:mcherry)* for selection (Kwan et al., 2007). The plasmid expressing the transgene was co-injected at 12-25 pg along with 50-100 pg of Tol2 transposase mRNA at 1-cell stage (Kwan et al., 2007). Injected embryos were selected for further analysis based on strong expression of mcherry in the heart by the cardiac reporter *Tg(cmlc2:mcherry).* The injected animals were raised, outcrossed to TL or *Tg(mpeg:GFP)* lines, and presence of stable expression of mcherry in the heart was confirmed prior to experiments and/or imaging.

Timecourse and timelapse experiments

Embryos for all timecourse and timelapse experiments were staged between 0 and 12 hpf and typically dechorionated between 30-36 hpf. For the 24-26 hpf timepoint, embryos were dechorionated immediately prior to mounting. For all timecourse and timelapse experiments, genotyping was done after counting and image acquisition using Zeiss LSM confocal microscope.

For all timecourse experiments, cells were first counted, and a single, high-resolution, representative plane was subsequently imaged using the 20X objective.

For the timelapse experiments starting at 60 hpf, a region of interest in the brain containing the midbrain, forebrain and a portion of the hindbrain was selected. All images were acquired using the 20X objective. The depth of acquisition was determined in each case individually; the most dorsal portion of the head containing macrophages was selected as the first plane and 10 z-slices, 2 μm apart were acquired, with an interval of 300 seconds per acquisition and a total of 100 imaging cycles. Following 17 hours 41 minutes of acquisition, maximum intensity projection of the z-slices was performed using the Zen Black software. For the purpose of analyses, macrophages within the brain were counted at each timepoint from the acquired images.

For the injury timelapse experiments, animals at 4 dpf were anesthetized and the tip of the tail fin was cut using a new scalpel ensuring approximately same size of incision in all animals. Immediately after injury, animals were mounted in 1.5% agarose with anesthetic, and timelapse imaging was performed for 8 hours post injury. All imaging was done using a 10X objective and 10 z-slices were selected, each slice 1 μm apart, at an interval of 300 seconds per acquisition. The number of macrophages at the site of injury was counted from maximum intensity projection of the z-slices.

LEGENDS

Figure 1: Defective macrophages in *rraga* mutants fail to colonize the brain. (A) images of *mpeg:GFP* expression in *rraga* mutant and heterozygous embryos between 24-26 hpf (lateral views of the head and yolk) (B, C) Quantitation of macrophages in yolk (B) and rest of the body (C). Each point represents the number of GFP^+ cells in a single embryo. (D) Dorsal views of *mpeg:GFP* expression at the indicated stages along with the corresponding quantification of developing microglia in the brain. (E-H) Timelapse imaging of *mpeg:GFP*$^+$ macrophages in the midbrain in *rraga* mutants and their siblings between 60 and ~78 hpf. (E) Representative images from timelapse movies (dorsal views, anterior on top). Images show maximum intensity projections of z-slices at indicated times. (F-H) Quantitative analysis of timelapse movies. In (F), each line shows macrophage cell counts from a single embryo over time. (I-L) Lateral views of macrophages and quantitation, in the head (I, I', K) and trunk+tail (J, J', L) in *rraga* mutants and their siblings. (M) High magnification images showing the difference in the morphology of macrophages between *rraga* mutant and heterozygous animals at 3 dpf. (N) Macrophage response to tail injury at 4 dpf. Arrows in the wildtype image show macrophages at the wound site (yellow dotted line). 2 dpf scale bars, 100 μm. All other scale bars, 50 μm. All graphs show mean with standard deviation; significance was determined using unpaired t-test.

Figure 2. Microglia numbers are restored in *rraga* mutants with simultaneous loss of *tfeb, tfe3a,* or *tfe3b.* Images show dorsal views of the midbrain (anterior on top) of

neutral red (NR) stained larvae of indicated genotypes at 5 dpf and graphs show corresponding quantification. (A, B) progeny from *rraga*$^{+/-}$; *tfeb*$^{+/-}$ intercross; (C, D) progeny from *rraga*$^{+/-}$; *tfe3a*$^{+/-}$ intercross; (E, F) progeny from *rraga*$^{+/-}$; *tfe3b*$^{+/-}$ intercross; and (G, H, I) progeny *rraga*$^{+/-}$; *tfeb*$^{+/-}$; *tfe3a*$^{+/-}$; *tfe3b*$^{+/-}$ quadruple heterozygous intercross. Images of a *rraga* mutant and *tfeb* and *tfe3* genotypes that result in complete rescue of NR^{+} microglia in *rraga* mutants are shown in (H). In (G), the same genotypes, but in a background wildtype for *rraga*, are included for comparison. Each point in the graph represents the number of microglia of a single animal. All graphs show mean with standard deviation; significance was determined using unpaired t-test.

Figure 3. Simultaneous mutation in *tfeb, tfe3a,* or *tfe3b* rescues *flcn* and *rraga* mutant phenotypes. (A) Neutral red assay and quantification of microglia in larvae obtained from *flcn*$^{+/-}$; *tfeb*$^{+/-}$; *tfe3b*$^{+/-}$ intercross. (B, C) LysoTracker Red assay and quantification of the area of LysoTracker Red punctae in microglia of larvae from (B) *rraga*$^{+/-}$; *tfe3a*$^{+/-}$ intercross and (C) *flcn*$^{+/-}$; *tfeb*$^{+/-}$; *tfe3b*$^{+/-}$ intercross. Images show LysoTracker Red signal in dorsal view of the midbrain. (D, E) *apoe* mRNA expression at 4 dpf and rescue of microglia in the progeny of (D) *rraga*$^{+/-}$; *tfe3a*$^{+/-}$ intercross, and (E) *flcn*$^{+/-}$; *tfeb*$^{+/-}$; *tfe3b*$^{+/-}$ intercross. (F, G) *mpeg:GFP* expression to visualize microglia and macrophages in (F) *rraga; tfe3a* double mutants and (G) *flcn; tfeb; tfe3b* triple mutants. Arrows denote microglia and macrophages in which ramified morphology has been restored, and asterisks denote cells with amoeboid morphology, insets show magnified views of cell morphology. Scale bars, 50 μm. All graphs show mean with standard deviation; significance was determined using unpaired t-test.

Figure 4. Overexpression of *tfe3b* in the macrophage lineage phenocopies *rraga* mutants. Comparison of macrophages and microglia between animals overexpressing Tfe3b in the macrophage lineage, *Tg(mpeg:tfe3b),* and controls, *Tg(mpeg:GFP)*. (A) Neutral red assay and quantification, (B) LysoTracker Red assay and quantification, (C) *apoe* in situ hybridization, and (D, E) live imaging with the *mpeg:GFP* transgene in (D) the brain and (E) head, yolk, and tail regions. Insets show magnified views of cell morphology. Scale bars, 50 μm. All graphs show mean with standard deviation; significance was determined using unpaired t-test.

AUTHOR CONTRIBUTIONS

H.I. and W.S.T designed the experiments and wrote the manuscript with input from all authors.

H.I., K.S., and A.M.M. performed the experiments.

ACKNOWLEDGMENTS

We thank Tuky Reyes and Chenelle Hill for maintaining the fish facility. We are grateful to Daniel Lysko, Mariapaola Sidoli, and Ellen Bouchard for their thoughtful comments on the manuscript. H.I. was supported by a fellowship from the American Heart Association (18POST33990334) and K.S. was supported by a fellowship from A*STAR Singapore. W.S.T. is a Catherine R. Kennedy and Daniel L. Grossman Fellow in Human Biology.

This work was supported by NIH grant R35NS111584 and NMSS grant RG-1707-28694 to W.S.T.

REFERENCES

Amit, I., Winter, D.R., and Jung, S. (2016). The role of the local environment and epigenetics in shaping macrophage identity and their effect on tissue homeostasis. Nat Immunol *17*, 18-25.
Block, M.L., Zecca, L., and Hong, J.S. (2007). Microglia-mediated neurotoxicity: uncovering the molecular mechanisms. Nat Rev Neurosci *8*, 57-69.
Bohlen, C.J., Bennett, F.C., Tucker, A.F., Collins, H.Y., Mulinyawe, S.B., and Barres, B.A. (2017). Diverse Requirements for Microglial Survival, Specification, and Function Revealed by Defined-Medium Cultures. Neuron *94*, 759-773 e758.
Butovsky, O., Jedrychowski, M.P., Moore, C.S., Cialic, R., Lanser, A.J., Gabriely, G., Koeglsperger, T., Dake, B., Wu, P.M., Doykan, C.E.*, et al.* (2014). Identification of a unique TGF-beta-dependent molecular and functional signature in microglia. Nat Neurosci *17*, 131-143.
Casano, A.M., Albert, M., and Peri, F. (2016). Developmental Apoptosis Mediates Entry and Positioning of Microglia in the Zebrafish Brain. Cell Rep *16*, 897-906.
Cortes, C.J., Miranda, H.C., Frankowski, H., Batlevi, Y., Young, J.E., Le, A., Ivanov, N., Sopher, B.L., Carromeu, C., Muotri, A.R.*, et al.* (2014). Polyglutamine-expanded androgen receptor interferes with TFEB to elicit autophagy defects in SBMA. Nat Neurosci *17*, 1180-1189.
Cunningham, C.L., Martinez-Cerdeno, V., and Noctor, S.C. (2013). Microglia regulate the number of neural precursor cells in the developing cerebral cortex. J Neurosci *33*, 4216-4233.
Davalos, D., Grutzendler, J., Yang, G., Kim, J.V., Zuo, Y., Jung, S., Littman, D.R., Dustin, M.L., and Gan, W.B. (2005). ATP mediates rapid microglial response to local brain injury in vivo. Nat Neurosci *8*, 752-758.
De Biase, L.M., Schuebel, K.E., Fusfeld, Z.H., Jair, K., Hawes, I.A., Cimbro, R., Zhang, H.Y., Liu, Q.R., Shen, H., Xi, Z.X.*, et al.* (2017). Local Cues Establish and Maintain Region-Specific Phenotypes of Basal Ganglia Microglia. Neuron *95*, 341-356 e346.
Decressac, M., Mattsson, B., Weikop, P., Lundblad, M., Jakobsson, J., and Bjorklund, A. (2013). TFEB-mediated autophagy rescues midbrain dopamine neurons from alpha-synuclein toxicity. Proc Natl Acad Sci U S A *110*, E1817-1826.
Dehay, B., Bove, J., Rodriguez-Muela, N., Perier, C., Recasens, A., Boya, P., and Vila, M. (2010). Pathogenic lysosomal depletion in Parkinson's disease. J Neurosci *30*, 12535-12544.
El-Houjeiri, L., Possik, E., Vijayaraghavan, T., Paquette, M., Martina, J.A., Kazan, J.M., Ma, E.H., Jones, R., Blanchette, P., Puertollano, R.*, et al.* (2019). The Transcription Factors TFEB and TFE3 Link the FLCN-AMPK Signaling Axis to Innate Immune Response and Pathogen Resistance. Cell Rep *26*, 3613-3628 e3616.
Ellett, F., Pase, L., Hayman, J.W., Andrianopoulos, A., and Lieschke, G.J. (2011). mpeg1 promoter transgenes direct macrophage-lineage expression in zebrafish. Blood *117*, e49-56.
Ferguson, S.M. (2015). Beyond indigestion: emerging roles for lysosome-based signaling in human disease. Curr Opin Cell Biol *35*, 59-68.

Ferrero, G., Mahony, C.B., Dupuis, E., Yvernogeau, L., Di Ruggiero, E., Miserocchi, M., Caron, M., Robin, C., Traver, D., Bertrand, J.Y.*, et al.* (2018). Embryonic Microglia Derive from Primitive Macrophages and Are Replaced by cmyb-Dependent Definitive Microglia in Zebrafish. Cell Rep *24*, 130-141.
Gosselin, D., Link, V.M., Romanoski, C.E., Fonseca, G.J., Eichenfield, D.Z., Spann, N.J., Stender, J.D., Chun, H.B., Garner, H., Geissmann, F.*, et al.* (2014). Environment drives selection and function of enhancers controlling tissue-specific macrophage identities. Cell *159*, 1327-1340.
Gosselin, D., Skola, D., Coufal, N.G., Holtman, I.R., Schlachetzki, J.C.M., Sajti, E., Jaeger, B.N., O'Connor, C., Fitzpatrick, C., Pasillas, M.P.*, et al.* (2017). An environment-dependent transcriptional network specifies human microglia identity. Science *356*.
Hagemeyer, N., Hanft, K.M., Akriditou, M.A., Unger, N., Park, E.S., Stanley, E.R., Staszewski, O., Dimou, L., and Prinz, M. (2017). Microglia contribute to normal myelinogenesis and to oligodendrocyte progenitor maintenance during adulthood. Acta Neuropathol *134*, 441-458.
Herbomel, P., Thisse, B., and Thisse, C. (1999). Ontogeny and behaviour of early macrophages in the zebrafish embryo. Development *126*, 3735-3745.
Herbomel, P., Thisse, B., and Thisse, C. (2001). Zebrafish early macrophages colonize cephalic mesenchyme and developing brain, retina, and epidermis through a M-CSF receptor-dependent invasive process. Dev Biol *238*, 274-288.
Holtman, I.R., Raj, D.D., Miller, J.A., Schaafsma, W., Yin, Z., Brouwer, N., Wes, P.D., Moller, T., Orre, M., Kamphuis, W.*, et al.* (2015). Induction of a common microglia gene expression signature by aging and neurodegenerative conditions: a co-expression meta-analysis. Acta Neuropathol Commun *3*, 31.
Hong, S.B., Oh, H., Valera, V.A., Baba, M., Schmidt, L.S., and Linehan, W.M. (2010). Inactivation of the FLCN tumor suppressor gene induces TFE3 transcriptional activity by increasing its nuclear localization. PLoS One *5*, e15793.
Kaplanis, J., Samocha, K.E., Wiel, L., Zhang, Z., Arvai, K.J., Eberhardt, R.Y., Gallone, G., Lelieveld, S.H., Martin, H.C., McRae, J.F.*, et al.* (2020). Evidence for 28 genetic disorders discovered by combining healthcare and research data. Nature.
Kwan, K.M., Fujimoto, E., Grabher, C., Mangum, B.D., Hardy, M.E., Campbell, D.S., Parant, J.M., Yost, H.J., Kanki, J.P., and Chien, C.B. (2007). The Tol2kit: a multisite gateway-based construction kit for Tol2 transposon transgenesis constructs. Dev Dyn *236*, 3088-3099.
Labun, K., Montague, T.G., Gagnon, J.A., Thyme, S.B., and Valen, E. (2016). CHOPCHOP v2: a web tool for the next generation of CRISPR genome engineering. Nucleic Acids Res *44*, W272-276.
Li, J., Wada, S., Weaver, L.K., Biswas, C., Behrens, E.M., and Arany, Z. (2019). Myeloid Folliculin balances mTOR activation to maintain innate immunity homeostasis. JCI Insight *5*.
Lister, J.A., Lane, B.M., Nguyen, A., and Lunney, K. (2011). Embryonic expression of zebrafish MiT family genes tfe3b, tfeb, and tfec. Dev Dyn *240*, 2529-2538.
Martina, J.A., Diab, H.I., Brady, O.A., and Puertollano, R. (2016). TFEB and TFE3 are novel components of the integrated stress response. EMBO J *35*, 479-495.
Martina, J.A., Diab, H.I., Li, H., and Puertollano, R. (2014). Novel roles for the MiTF/TFE family of transcription factors in organelle biogenesis, nutrient sensing, and energy homeostasis. Cell Mol Life Sci *71*, 2483-2497.

Martina, J.A., and Puertollano, R. (2017). TFEB and TFE3: The art of multi-tasking under stress conditions. Transcription *8*, 48-54.
Martini-Stoica, H., Xu, Y., Ballabio, A., and Zheng, H. (2016). The Autophagy-Lysosomal Pathway in Neurodegeneration: A TFEB Perspective. Trends Neurosci *39*, 221-234.
Matcovitch-Natan, O., Winter, D.R., Giladi, A., Vargas Aguilar, S., Spinrad, A., Sarrazin, S., Ben-Yehuda, H., David, E., Zelada Gonzalez, F., Perrin, P.*, et al.* (2016). Microglia development follows a stepwise program to regulate brain homeostasis. Science *353*, aad8670.
Mazzolini, J., Le Clerc, S., Morisse, G., Coulonges, C., Kuil, L.E., van Ham, T.J., Zagury, J.F., and Sieger, D. (2019). Gene expression profiling reveals a conserved microglia signature in larval zebrafish. Glia.
Meireles, A.M., Shen, K., Zoupi, L., Iyer, H., Bouchard, E.L., Williams, A., and Talbot, W.S. (2018). The Lysosomal Transcription Factor TFEB Represses Myelination Downstream of the Rag-Ragulator Complex. Dev Cell *47*, 319-330 e315.
Meireles, A.M., Shiau, C.E., Guenther, C.A., Sidik, H., Kingsley, D.M., and Talbot, W.S. (2014). The phosphate exporter xpr1b is required for differentiation of tissue-resident macrophages. Cell Rep *8*, 1659-1667.
Montague, T.G., Cruz, J.M., Gagnon, J.A., Church, G.M., and Valen, E. (2014). CHOPCHOP: a CRISPR/Cas9 and TALEN web tool for genome editing. Nucleic Acids Res *42*, W401-407.
Napolitano, G., and Ballabio, A. (2016). TFEB at a glance. J Cell Sci *129*, 2475-2481.
Nimmerjahn, A., Kirchhoff, F., and Helmchen, F. (2005). Resting microglial cells are highly dynamic surveillants of brain parenchyma in vivo. Science *308*, 1314-1318.
Nookala, R.K., Langemeyer, L., Pacitto, A., Ochoa-Montano, B., Donaldson, J.C., Blaszczyk, B.K., Chirgadze, D.Y., Barr, F.A., Bazan, J.F., and Blundell, T.L. (2012). Crystal structure of folliculin reveals a hidDENN function in genetically inherited renal cancer. Open Biol *2*, 120071.
Palmieri, M., Impey, S., Kang, H., di Ronza, A., Pelz, C., Sardiello, M., and Ballabio, A. (2011). Characterization of the CLEAR network reveals an integrated control of cellular clearance pathways. Hum Mol Genet *20*, 3852-3866.
Parr, C., Carzaniga, R., Gentleman, S.M., Van Leuven, F., Walter, J., and Sastre, M. (2012). Glycogen synthase kinase 3 inhibition promotes lysosomal biogenesis and autophagic degradation of the amyloid-beta precursor protein. Mol Cell Biol *32*, 4410-4418.
Pastore, N., Brady, O.A., Diab, H.I., Martina, J.A., Sun, L., Huynh, T., Lim, J.A., Zare, H., Raben, N., Ballabio, A.*, et al.* (2016). TFEB and TFE3 cooperate in the regulation of the innate immune response in activated macrophages. Autophagy *12*, 1240-1258.
Peri, F., and Nusslein-Volhard, C. (2008). Live imaging of neuronal degradation by microglia reveals a role for v0-ATPase a1 in phagosomal fusion in vivo. Cell *133*, 916-927.
Petit, C.S., Roczniak-Ferguson, A., and Ferguson, S.M. (2013). Recruitment of folliculin to lysosomes supports the amino acid-dependent activation of Rag GTPases. J Cell Biol *202*, 1107-1122.
Pickrell, A.M., and Youle, R.J. (2015). The roles of PINK1, parkin, and mitochondrial fidelity in Parkinson's disease. Neuron *85*, 257-273.
Plaza-Zabala, A., Sierra-Torre, V., and Sierra, A. (2017). Autophagy and Microglia: Novel Partners in Neurodegeneration and Aging. Int J Mol Sci *18*.

Polito, V.A., Li, H., Martini-Stoica, H., Wang, B., Yang, L., Xu, Y., Swartzlander, D.B., Palmieri, M., di Ronza, A., Lee, V.M.*, et al.* (2014). Selective clearance of aberrant tau proteins and rescue of neurotoxicity by transcription factor EB. EMBO Mol Med *6*, 1142-1160.
Raben, N., and Puertollano, R. (2016). TFEB and TFE3: Linking Lysosomes to Cellular Adaptation to Stress. Annu Rev Cell Dev Biol *32*, 255-278.
Reddy, K., Cusack, C.L., Nnah, I.C., Khayati, K., Saqcena, C., Huynh, T.B., Noggle, S.A., Ballabio, A., and Dobrowolski, R. (2016). Dysregulation of Nutrient Sensing and CLEARance in Presenilin Deficiency. Cell Rep *14*, 2166-2179.
Rossi, F., Casano, A.M., Henke, K., Richter, K., and Peri, F. (2015). The SLC7A7 Transporter Identifies Microglial Precursors prior to Entry into the Brain. Cell Rep *11*, 1008-1017.
Sardiello, M., Palmieri, M., di Ronza, A., Medina, D.L., Valenza, M., Gennarino, V.A., Di Malta, C., Donaudy, F., Embrione, V., Polishchuk, R.S.*, et al.* (2009). A gene network regulating lysosomal biogenesis and function. Science *325*, 473-477.
Schafer, D.P., Lehrman, E.K., Kautzman, A.G., Koyama, R., Mardinly, A.R., Yamasaki, R., Ransohoff, R.M., Greenberg, M.E., Barres, B.A., and Stevens, B. (2012). Microglia sculpt postnatal neural circuits in an activity and complement-dependent manner. Neuron *74*, 691-705.
Settembre, C., Di Malta, C., Polito, V.A., Garcia Arencibia, M., Vetrini, F., Erdin, S., Erdin, S.U., Huynh, T., Medina, D., Colella, P.*, et al.* (2011). TFEB links autophagy to lysosomal biogenesis. Science *332*, 1429-1433.
Settembre, C., Fraldi, A., Medina, D.L., and Ballabio, A. (2013). Signals from the lysosome: a control centre for cellular clearance and energy metabolism. Nat Rev Mol Cell Biol *14*, 283-296.
Shen, K., Sidik, H., and Talbot, W.S. (2016). The Rag-Ragulator Complex Regulates Lysosome Function and Phagocytic Flux in Microglia. Cell Rep *14*, 547-559.
Shiau, C.E., Monk, K.R., Joo, W., and Talbot, W.S. (2013). An anti-inflammatory NOD-like receptor is required for microglia development. Cell Rep *5*, 1342-1352.
Shigemoto-Mogami, Y., Hoshikawa, K., Goldman, J.E., Sekino, Y., and Sato, K. (2014). Microglia enhance neurogenesis and oligodendrogenesis in the early postnatal subventricular zone. J Neurosci *34*, 2231-2243.
Sierra, A., Encinas, J.M., Deudero, J.J., Chancey, J.H., Enikolopov, G., Overstreet-Wadiche, L.S., Tsirka, S.E., and Maletic-Savatic, M. (2010). Microglia shape adult hippocampal neurogenesis through apoptosis-coupled phagocytosis. Cell Stem Cell *7*, 483-495.
Sole-Domenech, S., Cruz, D.L., Capetillo-Zarate, E., and Maxfield, F.R. (2016). The endocytic pathway in microglia during health, aging and Alzheimer's disease. Ageing Res Rev *32*, 89-103.
Thisse, C., and Thisse, B. (2008). High-resolution in situ hybridization to whole-mount zebrafish embryos. Nat Protoc *3*, 59-69.
Tsun, Z.Y., Bar-Peled, L., Chantranupong, L., Zoncu, R., Wang, T., Kim, C., Spooner, E., and Sabatini, D.M. (2013). The folliculin tumor suppressor is a GAP for the RagC/D GTPases that signal amino acid levels to mTORC1. Mol Cell *52*, 495-505.
Tsunemi, T., Ashe, T.D., Morrison, B.E., Soriano, K.R., Au, J., Roque, R.A., Lazarowski, E.R., Damian, V.A., Masliah, E., and La Spada, A.R. (2012). PGC-1alpha rescues Huntington's disease proteotoxicity by preventing oxidative stress and promoting TFEB function. Sci Transl Med *4*, 142ra197.

Villegas, F., Lehalle, D., Mayer, D., Rittirsch, M., Stadler, M.B., Zinner, M., Olivieri, D., Vabres, P., Duplomb-Jego, L., De Bont, E.*, et al.* (2019). Lysosomal Signaling Licenses Embryonic Stem Cell Differentiation via Inactivation of Tfe3. Cell Stem Cell *24*, 257-270 e258.
Wada, S., Neinast, M., Jang, C., Ibrahim, Y.H., Lee, G., Babu, A., Li, J., Hoshino, A., Rowe, G.C., Rhee, J.*, et al.* (2016). The tumor suppressor FLCN mediates an alternate mTOR pathway to regulate browning of adipose tissue. Genes Dev *30*, 2551-2564.
Wakselman, S., Bechade, C., Roumier, A., Bernard, D., Triller, A., and Bessis, A. (2008). Developmental neuronal death in hippocampus requires the microglial CD11b integrin and DAP12 immunoreceptor. J Neurosci *28*, 8138-8143.
Wu, S., Xue, R., Hassan, S., Nguyen, T.M.L., Wang, T., Pan, H., Xu, J., Liu, Q., Zhang, W., and Wen, Z. (2018). Il34-Csf1r Pathway Regulates the Migration and Colonization of Microglial Precursors. Dev Cell *46*, 552-563 e554.
Xiao, Q., Yan, P., Ma, X., Liu, H., Perez, R., Zhu, A., Gonzales, E., Burchett, J.M., Schuler, D.R., Cirrito, J.R.*, et al.* (2014). Enhancing astrocytic lysosome biogenesis facilitates Abeta clearance and attenuates amyloid plaque pathogenesis. J Neurosci *34*, 9607-9620.
Xiao, Q., Yan, P., Ma, X., Liu, H., Perez, R., Zhu, A., Gonzales, E., Tripoli, D.L., Czerniewski, L., Ballabio, A.*, et al.* (2015). Neuronal-Targeted TFEB Accelerates Lysosomal Degradation of APP, Reducing Abeta Generation and Amyloid Plaque Pathogenesis. J Neurosci *35*, 12137-12151.
Xu, J., Wang, T., Wu, Y., Jin, W., and Wen, Z. (2016). Microglia Colonization of Developing Zebrafish Midbrain Is Promoted by Apoptotic Neuron and Lysophosphatidylcholine. Dev Cell *38*, 214-222.
Xu, J., Zhu, L., He, S., Wu, Y., Jin, W., Yu, T., Qu, J.Y., and Wen, Z. (2015). Temporal-Spatial Resolution Fate Mapping Reveals Distinct Origins for Embryonic and Adult Microglia in Zebrafish. Dev Cell *34*, 632-641.

Figure 1

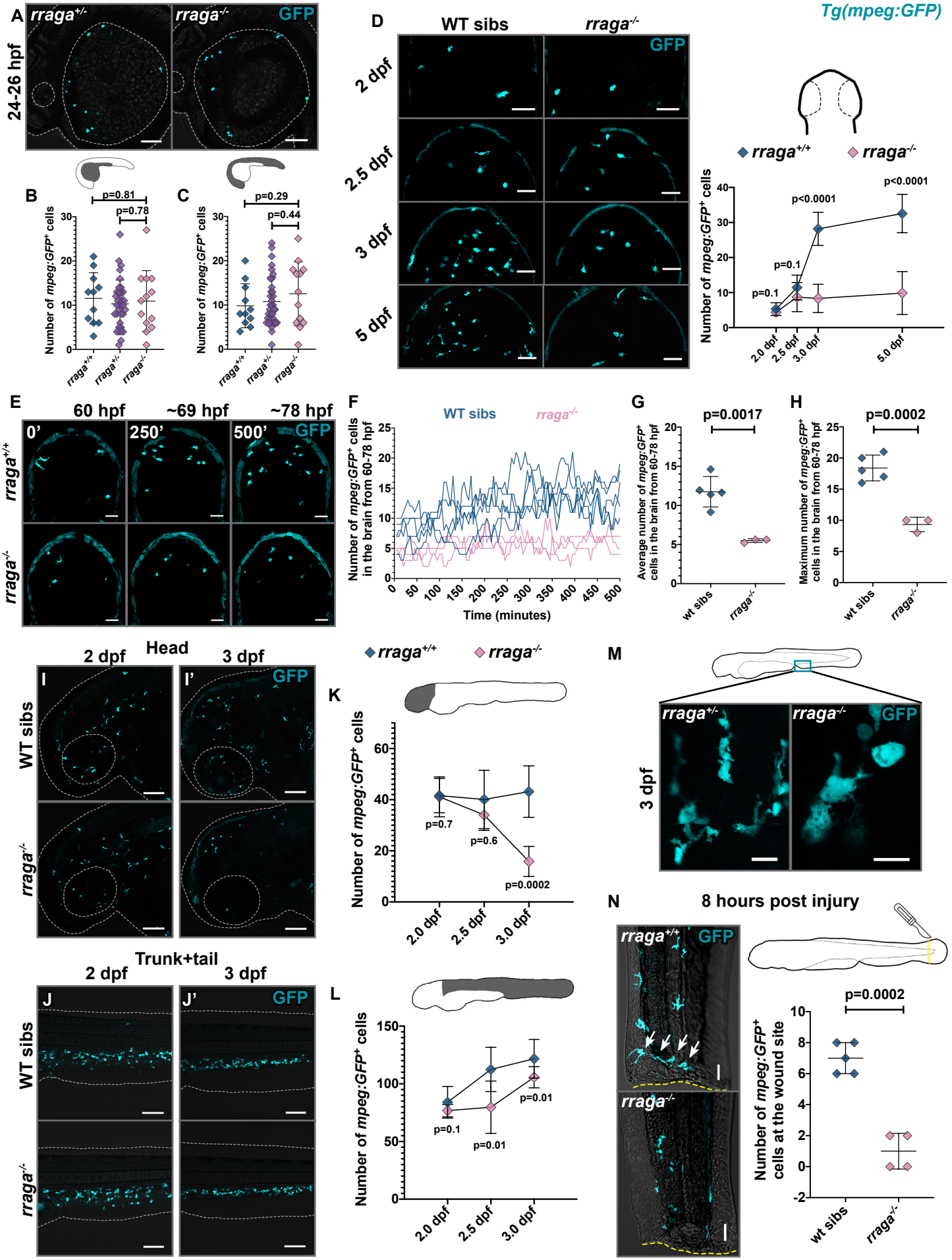
A
rraga+/-
rraga-/-
GFP
24-26 hpf
B
p=0.81
p=0.78
Number of mpeg:GFP+ cells
rraga+/+
rraga+/-
rraga-/-
C
p=0.29
p=0.44
D
WT sibs
rraga-/-
GFP
2 dpf
2.5 dpf
3 dpf
5 dpf
Tg(mpeg:GFP)
rraga+/+
rraga-/-
p<0.0001
p<0.0001
p=0.1
p=0.1
2.0 dpf
2.5 dpf
3.0 dpf
5.0 dpf
E
60 hpf
~69 hpf
~78 hpf
0'
250'
500'
F
WT sibs
rraga-/-
Number of mpeg:GFP+ cells in the brain from 60-78 hpf
Time (minutes)
G
p=0.0017
Average number of mpeg:GFP+ cells in the brain from 60-78 hpf
wt sibs
H
p=0.0002
Maximum number of mpeg:GFP+ cells in the brain from 60-78 hpf
Head
2 dpf
3 dpf
I
I'
WT sibs
K
p=0.7
p=0.6
p=0.0002
M
3 dpf
Trunk+tail
J
J'
L
p=0.1
p=0.01
p=0.01
N
8 hours post injury
p=0.0002
Number of mpeg:GFP+ cells at the wound site

Figure 2

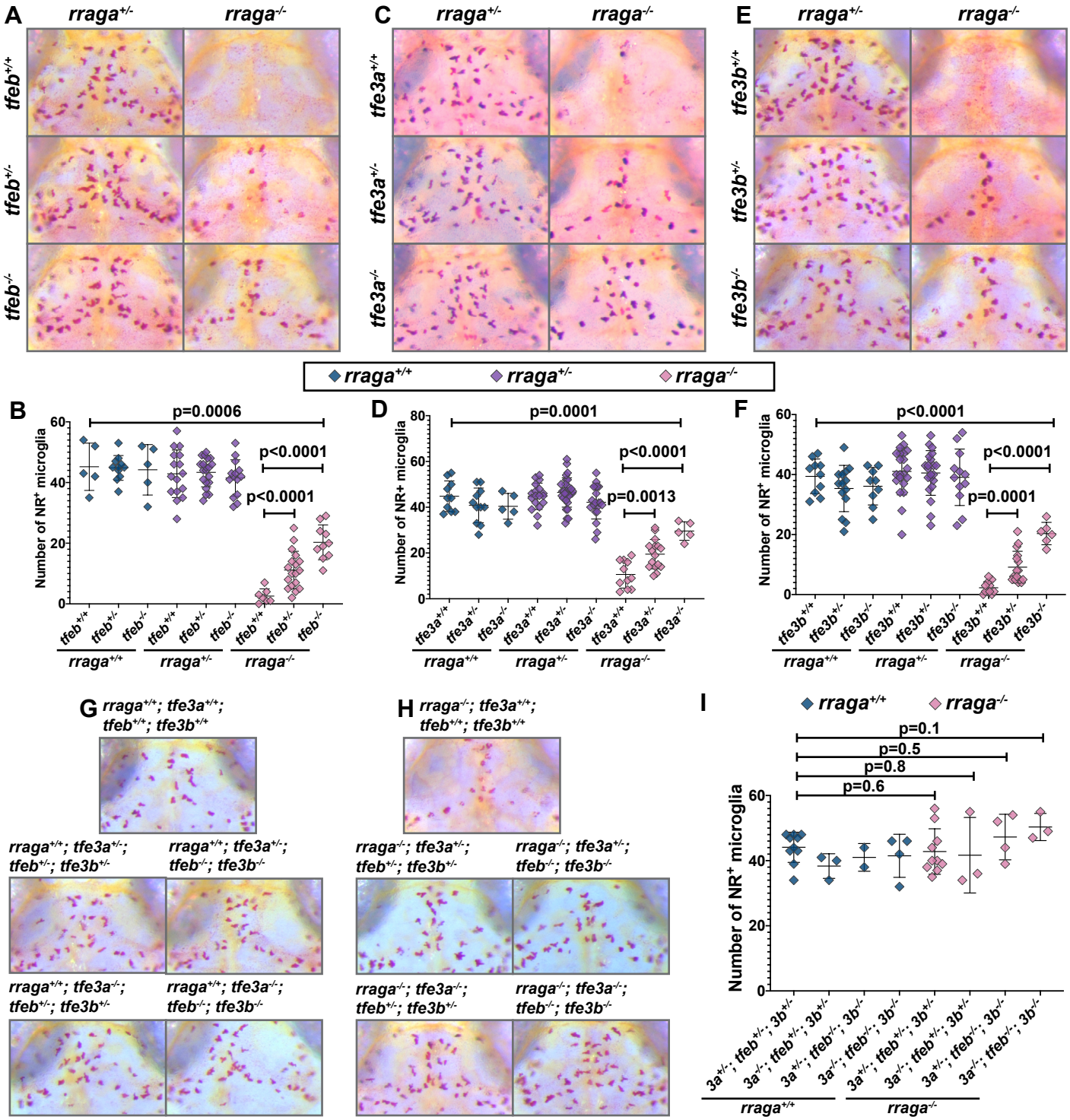
A
rraga+/-
rraga-/-
tfeb+/+
tfeb+/-
tfeb-/-
C
tfe3a+/+
tfe3a+/-
tfe3a-/-
E
tfe3b+/+
tfe3b+/-
tfe3b-/-
rraga+/+
rraga+/-
rraga-/-
B
Number of NR+ microglia
p=0.0006
p<0.0001
p<0.0001
D
p=0.0001
p<0.0001
p=0.0013
F
p<0.0001
p<0.0001
p=0.0001
G rraga+/+; tfe3a+/+; tfeb+/+; tfe3b+/+
rraga+/+; tfe3a+/-; tfeb+/-; tfe3b+/-
rraga+/+; tfe3a+/-; tfeb-/-; tfe3b-/-
rraga+/+; tfe3a-/-; tfeb+/-; tfe3b+/-
rraga+/+; tfe3a-/-; tfeb-/-; tfe3b-/-
H rraga-/-; tfe3a+/+; tfeb+/+; tfe3b+/+
rraga-/-; tfe3a+/-; tfeb+/-; tfe3b+/-
rraga-/-; tfe3a+/-; tfeb-/-; tfe3b-/-
rraga-/-; tfe3a-/-; tfeb+/-; tfe3b+/-
rraga-/-; tfe3a-/-; tfeb-/-; tfe3b-/-
I
p=0.1
p=0.5
p=0.8
p=0.6
3a+/-; tfeb+/-; 3b+/-
3a-/-; tfeb+/-; 3b+/-
3a+/-; tfeb-/-; 3b-/-
3a-/-; tfeb-/-; 3b-/-
3a+/-; tfeb+/-; 3b+/-
3a-/-; tfeb+/-; 3b+/-
3a+/-; tfeb-/-; 3b-/-
3a-/-; tfeb-/-; 3b-/-

Figure 3

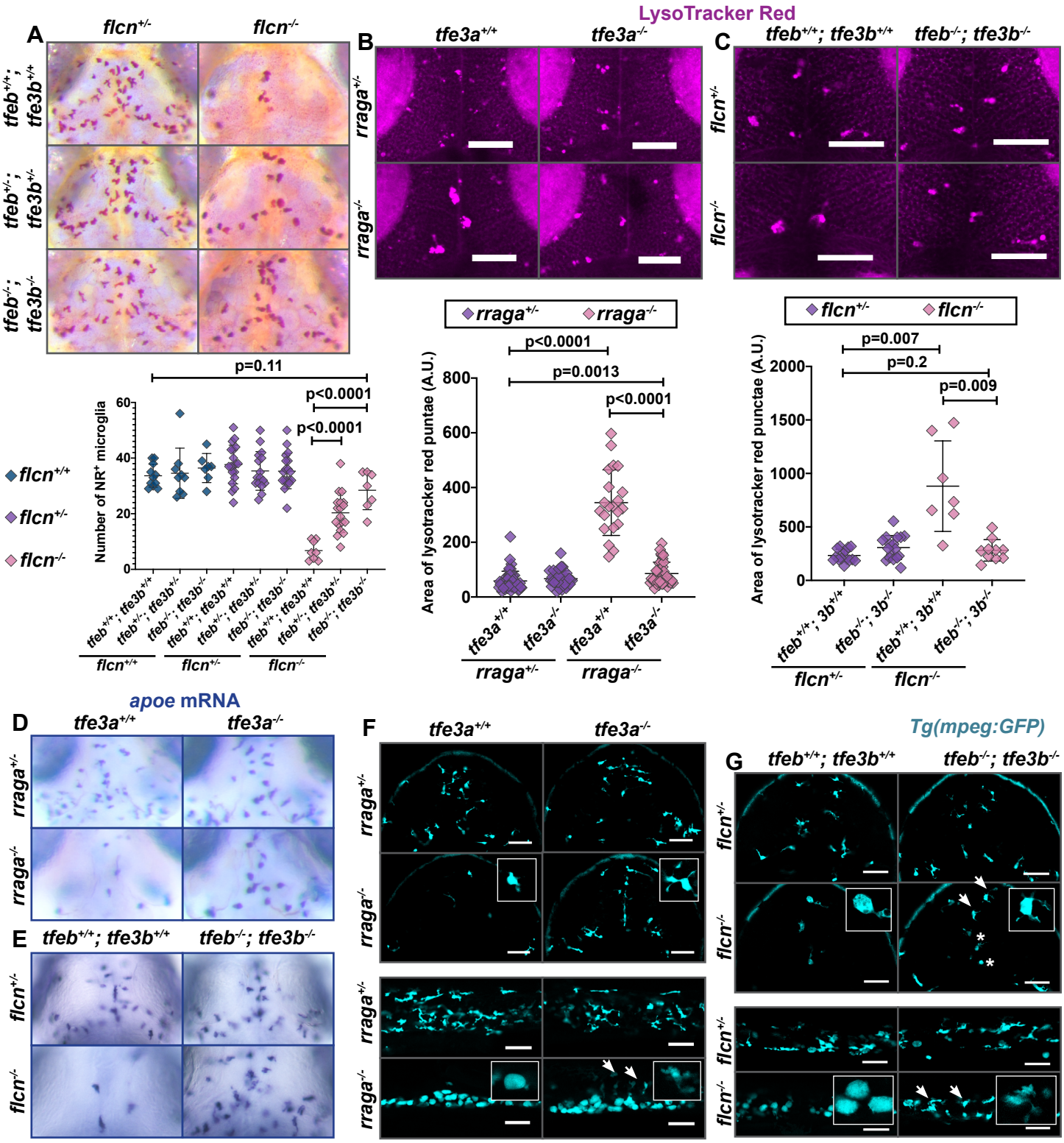
A
flcn+/-
flcn-/-
tfeb+/+; tfe3b+/+
tfeb+/-; tfe3b+/-
tfeb-/-; tfe3b-/-
LysoTracker Red
B
tfe3a+/+
tfe3a-/-
rraga+/-
rraga-/-
C
tfeb+/+; tfe3b+/+
tfeb-/-; tfe3b-/-
flcn+/-
flcn-/-
p=0.11
p<0.0001
p<0.0001
Number of NR+ microglia
flcn+/+
flcn+/-
flcn-/-
tfeb+/+; tfe3b+/+
tfeb+/-; tfe3b+/-
tfeb-/-; tfe3b-/-
rraga+/-
rraga-/-
p<0.0001
p=0.0013
p<0.0001
Area of lysotracker red puntae (A.U.)
tfe3a+/+
tfe3a-/-
p=0.007
p=0.2
p=0.009
Area of lysotracker red punctae (A.U.)
tfeb+/+; 3b+/+
tfeb-/-; 3b-/-
apoe mRNA
D
E
F
Tg(mpeg:GFP)
G

Figure 4

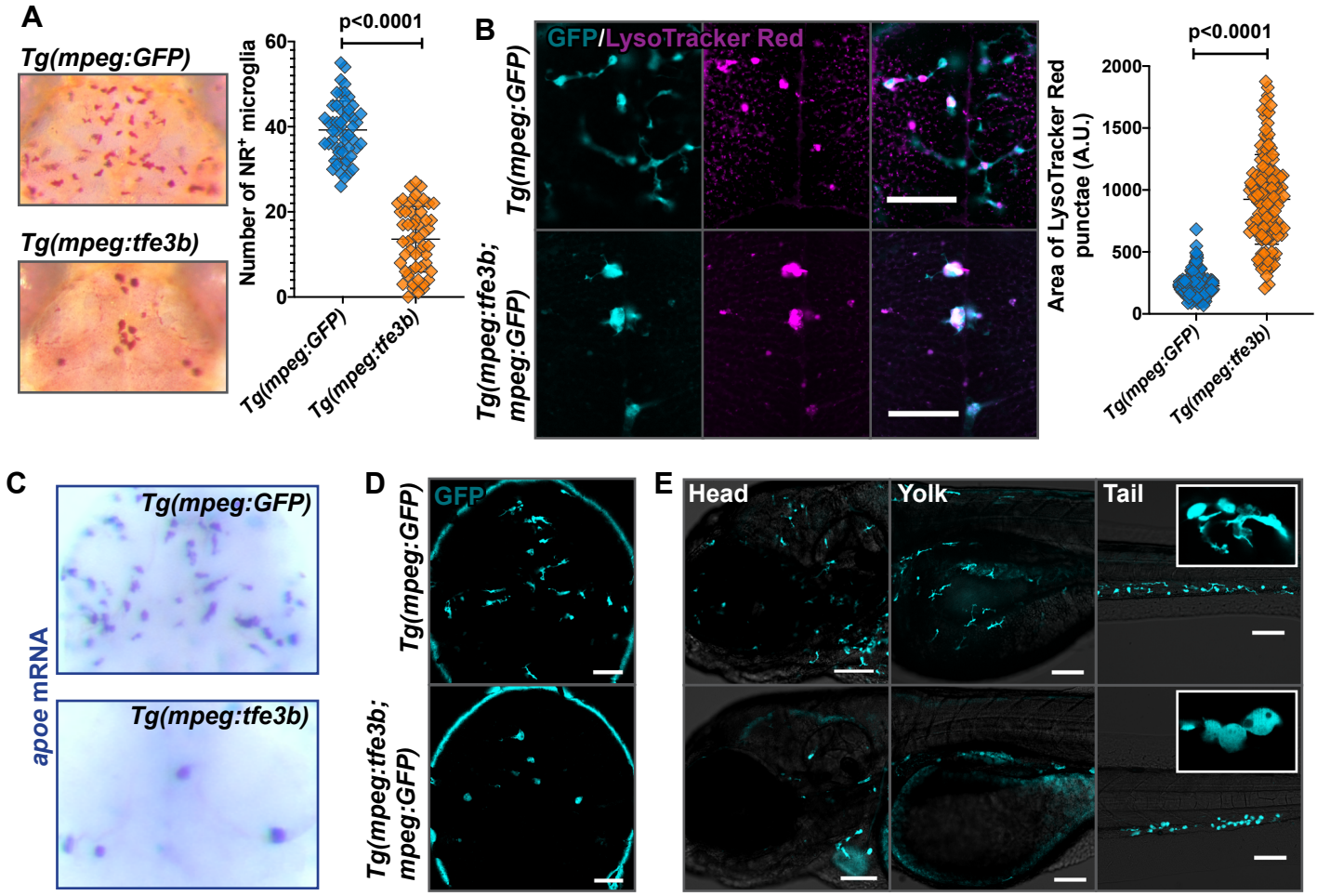
A
Tg(mpeg:GFP)
Tg(mpeg:tfe3b)
p<0.0001
Number of NR+ microglia
60
40
20
0
Tg(mpeg:GFP)
Tg(mpeg:tfe3b)
B
GFP/LysoTracker Red
Tg(mpeg:GFP)
Tg(mpeg:tfe3b; mpeg:GFP)
p<0.0001
Area of LysoTracker Red punctae (A.U.)
2000
1500
1000
500
0
Tg(mpeg:GFP)
Tg(mpeg:tfe3b)
C
apoe mRNA
Tg(mpeg:GFP)
Tg(mpeg:tfe3b)
D
GFP
Tg(mpeg:GFP)
Tg(mpeg:tfe3b; mpeg:GFP)
E
Head
Yolk
Tail